Chemical Engineering Journal 146 (2009) 307–314

Contents lists available at ScienceDirect

Chemical Engineering Journal

journal homepage: www.elsevier.com/locate/cej

Effect of calcination temperature of alumina supports on the wax hydrocracking performance of Pd-loaded mesoporous alumina xerogel catalysts for the production of middle distillate

Kyung Min Cho[a], Sunyoung Park[a], Jeong Gil Seo[a], Min Hye Youn[a], Insung Nam[a], Sung-Hyeon Baeck[b], Jin Suk Chung[c], Ki-Won Jun[d], In Kyu Song[a,*]

[a] School of Chemical and Biological Engineering, Institute of Chemical Processes, Seoul National University, Shinlim-dong, Kwanak-ku, Seoul 151-744, South Korea
[b] Department of Chemical Engineering, Inha University, Incheon 402-751, South Korea
[c] School of Chemical Engineering and Bioengineering, University of Ulsan, Ulsan 680-749, South Korea
[d] Korea Research Institute of Chemical Technology, Daejeon 305-600, South Korea

ARTICLE INFO

Article history:
Received 30 July 2008
Received in revised form 12 October 2008
Accepted 13 October 2008

Keywords:
Synthetic fuel
Middle distillate
Hydrocracking
Mesoporous alumina xerogel

ABSTRACT

Selective production of middle distillate (C_{10}–C_{20}) from synthesis gas ($CO + H_2$) through wax hydrocracking was carried out in a dual-bed reactor. Co/TiO_2 catalyst was used in the first-bed reactor to produce wax (C_{21+}) from synthesis gas, and Pd-loaded mesoporous alumina xerogel (denoted as Pd/XA) catalysts were used in the second-bed reactor to produce middle distillate through wax hydrocracking. The effect of calcination temperature of mesoporous alumina xerogel supports on the wax hydrocracking performance of Pd/XA catalysts was investigated. The increment of middle distillate selectivity increased with increasing medium acidity of Pd/XA catalyst. Among the Pd/XA catalysts, the Pd catalyst loaded on mesoporous alumina xerogel support calcined at 800 °C retained the highest medium acidity, and at the same time, showed the best catalytic performance in the hydrocracking of wax.

1. Introduction

Hydrocracking is a key process in petroleum refining for the conversion of heavy hydrocarbons into high value and low-boiling point products such as gasoline, diesel, and jet fuel [1–3]. Hydrocracking is also considered as a flexible process, because it allows the conversion of a wide range of feedstocks to a variety of products [2]. The hydrocracking reaction has been extensively studied in the hybrid Fischer–Tropsch synthesis for the production of gasoline (C_5–C_{11}) and middle distillate (C_{10}–C_{20}) [4–12].

Fischer–Tropsch synthesis (FTS) is a well-known process for producing high-quality fuels and petrochemicals from synthesis gas ($CO + H_2$) which can be easily obtained from other organic resources such as coal, biomass, and natural gas. Recently, FTS has been spotlighted as one of the major gas conversion routes for gas-to-liquid (GTL), coal-to-liquid (CTL), and biomass-to-liquid (BTL) processes [4,13,14]. FTS over conventional supported metal catalysts yields a wide spectrum of hydrocarbons, because the product distribution is controlled by the Anderson–Schulz–Flory (ASF) polymerization kinetics [4,13,15,16]. This imposes a limitation on the maximum selectivity for a given hydrocarbon product. It is known that the theoretical maximum selectivity for gasoline (C_5–C_{11}) is ca. 48%, while that for middle distillate (C_{10}–C_{20}) is ca. 40% [15,17]. In order to overcome the limitation of ASF distribution in the FTS, several hybrid FTS systems have been developed [16,18–21]. The hybrid FTS catalyst is composed of a typical Fischer–Tropsch (FT) catalyst and an acid catalyst. The function of acid catalyst in the hybrid FTS is to convert long-chain paraffins (FT products) into the desired products through hydrocracking reaction [16,18]. It has been reported that high yield for middle distillate can be obtained through wax hydrocracking in a dual-bed hybrid FT process [12,14]. The hydrocracking of FT wax yields high-quality diesel with cetane number of ca. 70 which is significantly higher than the minimum required value (ca. 51) for conventional diesel [1]. Furthermore, diesel fuel obtained from FTS retains extremely low sulfur and aromatic compounds, high-cetane index, and clean burning feature in compression-ignition engines [12]. FTS diesel fuel also shows low emission of carbon monoxide, nitrogen oxides, hydrocarbons, and other particulates. Thus, FTS diesel has been considered as a green fuel.

The dual-bed reactor system is composed of two serial reactions; a low-temperature FTS over Co-based catalyst for the production of long-chain *n*-paraffin (wax) in the first-bed reactor, and a subsequent hydrocracking of wax into middle distillate in the second-bed

* Corresponding author. Tel.: +82 2 880 9227; fax: +82 2 889 7415.
E-mail address: inksong@snu.ac.kr (I.K. Song).

1385-8947/$ – see front matter © 2008 Elsevier B.V. All rights reserved.
doi:10.1016/j.cej.2008.10.008

reactor [10]. In the dual-bed reactor system, the FTS reaction in the first-bed reactor and the hydrocracking reaction in the second-bed reactor are operated independently. Therefore, it is possible to control the product distribution by changing the reaction conditions.

It is known that the hydrocracking is generally conducted over a metal/acid bifunctional catalyst. Alkanes are dehydrogenated on the metallic sites and then isomerized or cracked on the acid sites through classical or non-classical carbenium ion chemistry [11,22–24]. The most conventional catalysts used for the production of diesel-range hydrocarbons are Ni–Mo and Ni–W oxides supported on alumina, alumina-silicates, and molecular sieves. In the hydrocracking of FT wax which is virtually free of sulfur (<5 ppm) and contains extremely low-aromatic compounds (<1 wt%) [1,3,25], noble metal-based catalysts (Pt- or Pd-loaded solid acid catalysts) have been employed, because these catalysts show a high-hydrogenation activity for hydrocracking of sulfur-free hydrocarbons. For the hydrocracking reaction in the dual-bed FTS, however, the Pd-loaded catalyst is known to be more suitable than the Pt-loaded catalyst. This is because the metallic function of Pd is not damaged by the co-adsorption of CO, while that of Pt is interrupted by molecularly adsorbed CO [4,26].

The catalytic performance of Pd-loaded catalyst in the hydrocracking reaction strongly depends on the chemical and textural properties of support. Therefore, modification of an appropriate support for Pd catalyst can be a feasible route to improve the catalytic performance of Pd-loaded catalyst in the hydrocracking reaction. Sol–gel synthesis has been recognized as an attractive method for the preparation of supported noble metal catalysts [27,28]. In particular, mesoporous alumina materials prepared by a sol–gel method have high-surface area and controllable mesopore, which is important to reduce the mass transfer resistance of heavy hydrocarbons in the hydrocracking reaction. It has also been reported that the mesoporous alumina xerogel support prepared by a sol–gel method retains strong resistance against coke deposition [29,30].

Acid property of support is also important to yield high selectivity for middle distillate in the hydrocracking of wax. It is known that alumina phase is transformed from boehmite (AlOOH) to γ-, δ-, θ-, and α-Al_2O_3 with increasing calcination temperature [31,32]. It has also been reported that the degree of crystallinity of alumina is related to the acidity of alumina [33]. Therefore, it is expected that the acidity of alumina support can be controlled by changing the calcination temperature.

In our previous work [12], the role and effect of mesoporous alumina xerogel support on the catalytic performance of supported catalyst in the hydrocracking reaction has been investigated. However, the effect of calcination temperature on the acidity of alumina xerogel support, and in turn, on the catalytic performance of supported catalyst in the hydrocracking of wax has never been reported yet. Therefore, developing an efficient sol–gel derived mesoporous alumina xerogel support for the second-bed hydrocracking catalyst would be of great interest.

In this work, mesoporous alumina xerogel (denoted as XA) supports prepared by a sol–gel method were calcined at various temperatures. Pd-loaded mesoporous alumina xerogel (denoted as Pd/XA) catalysts were then prepared by an impregnation method for use in the production of middle distillate from wax through hydrocracking in the second-bed reactor. The effect of calcination temperature of XA supports on the wax hydrocracking performance of Pd/XA catalysts to produce middle distillate in the second-bed reactor was investigated. Co/TiO_2 catalyst prepared by an incipient wetness impregnation method was used as an efficient FTS catalyst for the production of wax from synthesis gas in the first-bed reactor [12].

2. Experimental

2.1. Preparation of Co/TiO_2 catalyst

15 wt% Co/TiO_2 was prepared by an incipient wetness impregnation method for use as a FTS catalyst in the first-bed reactor. Cobalt nitrate ($Co(NO_3)_2{\cdot}6H_2O$, Sigma–Aldrich) was used as a cobalt precursor, and TiO_2 (P25, Degussa) was used as a support. The prepared Co/TiO_2 catalyst was calcined at 300 °C for 20 h [34].

2.2. Preparation of Pd/XA catalyst

Mesoporous alumina xerogel (XA) supports were prepared according to the reported method [29]. A known amount of aluminum precursor (aluminum *sec*-butoxide, Sigma–Aldrich) was dissolved in ethanol at 80 °C with vigorous stirring. For the partial hydrolysis of aluminum precursor, small amounts of nitric acid and distilled water, which had been diluted with ethanol, were slowly added to the solution containing the aluminum precursor. After maintaining the resulting solution at 80 °C for a few minutes, a clear sol was obtained. The sol was then cooled to room temperature with vigorous stirring. Upon addition of an appropriate amount of water diluted with ethanol to the sol, a transparent monolithic gel was formed within a few minutes. The alumina gel was aged for 48 h and dried overnight at 100 °C. The dried alumina xerogel was calcined at 700, 750, 800, 850, 900, and 1000 °C for 5 h (denoted as XA700, XA750, XA800, XA850, XA900, and XA1000, respectively).

Pd/XA catalysts were prepared by an impregnation method using a known amount of palladium precursor ($Pd(NO_3)_2$, Sigma–Aldrich). The Pd loading on XA support was fixed at 1 wt% in all cases. After drying the impregnated catalysts overnight at 100 °C, they were calcined at 500 °C for 5 h. The prepared catalysts were denoted as Pd/XA700, Pd/XA750, Pd/XA800, Pd/XA850, Pd/XA900, and Pd/XA1000.

2.3. Characterization

Nitrogen adsorption–desorption isotherms of XA supports and Pd/XA catalysts were obtained with an ASAP-2010 (Micrometrics) instrument, and pore size distributions were determined by the Barret-Joyner-Hallender (BJH) method applied to the desorption branch of the isotherms. Crystalline phases of XA supports were investigated by XRD measurements (MAC Science, M18XHF-SRA) using Cu Kα radiation (λ = 1.54056 Å) operated at 50 kV and 100 mA. Surface morphology of XA supports and Pd dispersion of Pd/XA catalysts were examined by TEM analyses (Jeol, JEM-2000EXII). Acid properties of Pd/XA catalysts were measured by NH_3-TPD experiments. Each catalyst (0.2 g) was charged into a tubular quartz reactor of the conventional TPD apparatus. The catalyst was pretreated at 400 °C for 3 h under a flow of hydrogen (5 ml min^{-1}) and helium (10 ml min^{-1}) in order to reduce the catalyst. 20 ml of NH_3 was then pulsed into the reactor every minute at room temperature under a flow of helium (5 ml min^{-1}), until the acid sites were saturated with NH_3. The physisorbed NH_3 was removed by evacuating the catalyst sample at 50 °C for 1 h. The furnace temperature was increased from room temperature to 1000 °C at a heating rate of 5 °C min^{-1} under a flow of helium (10 ml min^{-1}). The desorbed NH_3 was detected using a GC equipped with a TCD (Younglin, ACME 6000).

2.4. Catalytic reaction

The reaction was carried out in a dual-bed fixed-bed reactor. Both first-bed and second-bed reactors (SUS, ID = 8 mm) were consecutively arranged in the vertical direction. In the first-bed reactor,

a FT catalyst (Co/TiO_2) was loaded to produce long-chain hydrocarbon (wax). In the second-bed reactor, a Pd/XA catalyst was loaded for hydrocracking of wax from the first-bed reactor. 0.3 g of Co/TiO_2 catalyst diluted with 0.5 g of quartz sand was charged in the first-bed reactor. The FTS reaction in the first-bed reactor was conducted under the conditions of $P = 12$ bar, $H_2/CO = 2.0$, $W/F = 20.0$ g-cat h mol^{-1}, and $T = 220\,^{\circ}C$. 0.3 g of Pd/XA catalyst was used in the second-bed reactor. Additional H_2 was introduced into the second-bed reactor, where H_2/CO ratio was fixed at 2.5 by assuming no reaction in the first-bed reactor. The reaction in the second-bed reactor was conducted under the condition of $P = 12$ bar and $T = 330\,^{\circ}C$. Prior to the reaction, Co/TiO_2 catalyst in the first-bed reactor was reduced at 250 °C for 16 h and Pd/XA catalyst in the second-bed reactor was reduced at 400 °C for 16 h. All the reaction experiments were conducted more than 24 h under the steady-state condition.

Effluent hydrocarbon products which were not condensed at a hot trap were analyzed using an on-line GC (HP 5890II, Agilent) equipped with a FID. CO, CH_4, and CO_2 in the effluent system from a water trap were analyzed using a GC (Younglin, 600D) equipped with a TCD, and light hydrocarbons (C_1–C_5) in the effluent stream were also analyzed using a GC (Younglin, 600D) equipped with a FID. Heavy hydrocarbon products (C_{10+}) collected from a hot trap were analyzed using a GC (HP 5890II, Agilent) equipped with a FID. The reaction data in each reactor were obtained after a 10-h reaction. For more accurate analysis, the liquid product was collected for 10 h without samplings. CO conversion and hydrocarbon selectivity were calculated according to the following equations:

$$\text{CO conversion (\%)} = \frac{\text{weight of CO introduced} - \text{weight of CO unreacted}}{\text{weight of CO introduced}} \times 100 \quad (1)$$

$$\text{Hydrocarbon selectivity (wt\%)} = \frac{\text{weight of specific hydrocarbon produced}}{\text{weight of total hydrocarbon produced}} \times 100 \quad (2)$$

3. Results and discussion

3.1. Textural property of supports and supported catalysts

Textural properties of XA supports and Pd/XA catalysts were examined by nitrogen adsorption–desorption isotherm measurements. Fig. 1 shows the nitrogen adsorption–desorption isotherms and pore size distributions of XA800 support and Pd/XA800 catalyst. Both XA800 and Pd/XA800 samples clearly showed IV-type isotherms with H2-type hysteresis loops, indicating the existence of well-developed framework mesopores [29,30]. All the other XA supports and Pd/XA catalysts also showed isotherms, hysteresis loops, and pore size distributions similar to those observed for XA800 support and Pd/XA800 catalyst. Average pore diameters of XA800 support and Pd/XA800 catalyst were 7.1 and 7.4 nm, respectively. The above results strongly support that the mesoporous structure of XA800 support was still maintained even after the impregnation of Pd on the support. Fig. 2 shows the TEM images of XA800 support and Pd/XA800 catalyst. The images showed that XA800 support retained well-developed mesopores as demonstrated in Fig. 1, and Pd species were finely dispersed in the Pd/XA800 catalyst. The above results indicate that Pd/XA catalysts with mesoporosity were successfully prepared in this work.

Surface areas, pore volumes, and average pore diameters of XA supports are summarized in Table 1. It is noticeable that

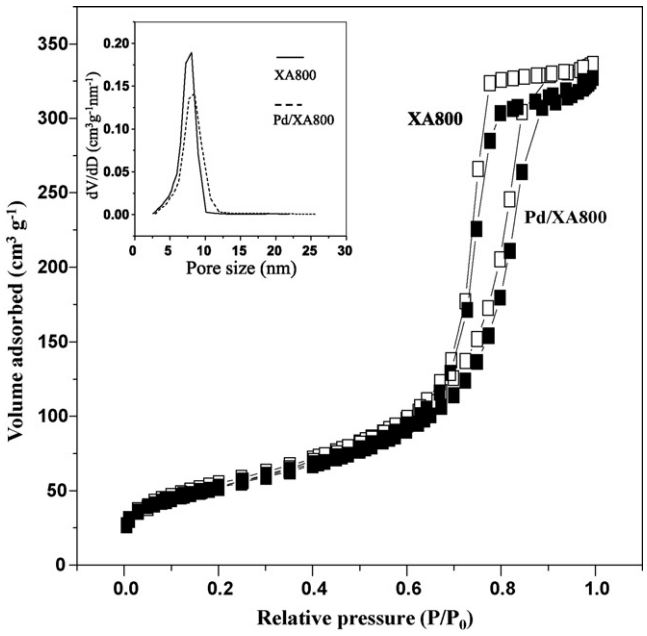

Fig. 1. Nitrogen adsorption–desorption isotherms and pore size distributions of XA800 support and Pd/XA800 catalyst.

surface area was decreased and pore volume was also roughly decreased with increasing calcination temperature of XA support, while average pore diameter was roughly increased with increasing calcination temperature. This implies the significant change in crystal structure of XA support depending on the calcination temperature. It is known that the surface area of alumina generally decreases with increasing calcination temperature due to the sintering and the phase transition to α-form [35,36]. It has also been reported that the increased pore size and the decreased pore volume with increasing calcination temperature are due to the change of wall crystal structure of alumina [37]. It is believed that boehmite (AlOOH), which contains only octahedrally coordinated aluminum and loses water to form tetrahedral Al_2O_3 upon annealing, was transformed into the transition state alumina such as γ-Al_2O_3 [31]. This was well confirmed by the following XRD measurements.

3.2. Crystal structure of XA supports

Fig. 3 shows the XRD patterns of XA supports. Although XA700 support showed amorphous-like feature, clear γ-Al_2O_3 phase started to appear in the XA750 support. This indicates that the transition of amorphous alumina into γ-Al_2O_3 occurred above 700 °C. It is known that the alumina phase is transformed from boehmite (AlOOH) to γ-Al_2O_3 at temperature of 400–500 °C [29,37,38]. In

Table 1
Textural properties of XA supports.

Support	Surface area ($m^2\ g^{-1}$)[a]	Pore volume ($cm^3\ g^{-1}$)[b]	Average pore diameter (nm)[c]
XA700	382	0.52	3.8
XA750	206	0.48	6.4
XA800	199	0.51	7.1
XA850	151	0.35	6.4
XA900	107	0.28	7.5
XA1000	68	0.24	10.1

[a] Calculated by the Brunauer–Emmett–Teller (BET) equation.
[b] BJH desorption pore volume.
[c] BJH desorption average pore diameter.

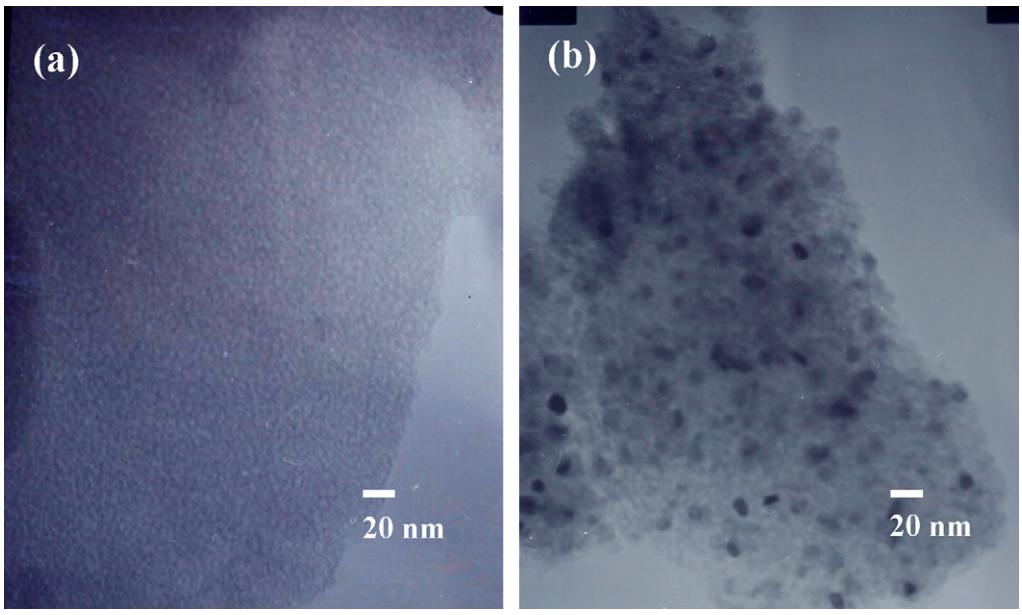

Fig. 2. TEM images of (a) XA800 support and (b) Pd/XA800 catalyst.

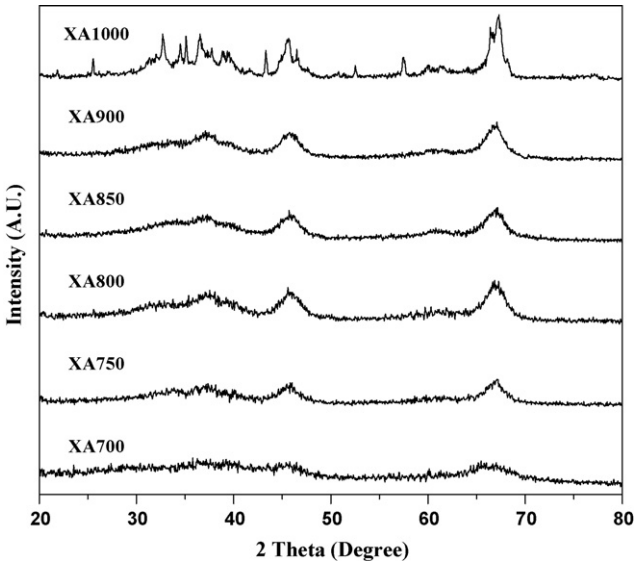

Fig. 3. XRD patterns of XA supports.

our experiments, however, it is believed that the hydroxyl-rich surface properties of alumina xerogel retarded the aggregation of alumina particles which might cause the phase transformation during the heat-treatment step [29]. XA750, XA 800, XA850, and XA900 supports showed almost the same XRD patterns, which were characteristic diffraction peaks of γ-Al_2O_3 [29]. On the other hand, the XRD patterns of XA1000 support were totally different from those of the other XA supports. This means that XA1000 is in the transition state between γ-Al_2O_3 and α-Al_2O_3, indicating the occurrence of phase transition between 900 and 1000 °C. Although this transition state may correspond to either δ-Al_2O_3 or θ-Al_2O_3, it was difficult to determine the accurate phase of XA1000 with the XRD patterns only. The diffraction peaks of XA1000 support were relatively sharp, indicating the formation of large crystals formed by vigorous sintering of boehmite in the XA1000 support.

3.3. Catalytic performance in the dual-bed reactor

It is desired to produce heavy hydrocarbons (middle distillate and wax) through FTS in the first-bed reactor. In this work, Co/TiO_2 was used as an efficient catalyst for the first-bed reactor [12,34]. As listed in Table 2, Co/TiO_2 catalyst showed high selectivities for middle distillate and wax enough to be used as a feed for the second-bed reactor. Co/TiO_2 catalyst in the first-bed reactor produced more than 35 wt% middle distillate and more than 25 wt% wax. These products could be utilized as a suitable feed for the production of middle distillate through hydrocracking in the second-bed reactor.

Fig. 4 shows the typical carbon number distributions of liquid product (C_{10+}) in the first-bed reactor (Co/TiO_2) and in the dual-bed reactor (Co/TiO_2 + Pd/XA800). Fig. 4 clearly shows that wax produced in the first-bed reactor was mainly hydrocracked to middle distillate. Selectivity for middle distillate in the dual-bed reactor was 12.9 wt% higher than that in the first-bed reactor. Such a product distribution was due to the hydrocracking of heavy hydrocarbons in the second-bed reactor. It has been reported that the intrinsic hydrocracking activity of *n*-paraffins increases with increasing carbon chain length [4,10,14,17]. It has also been reported that long-chain hydrocarbons (carbon number more than 20) have extremely high degree of adsorption on the catalyst surface [10], and therefore, selective hydrocracking of heavy hydrocarbons can occur. It can be said that all these led to the increment of mid-

Table 2
Catalytic activity of Co/TiO_2 for FTS in the first-bed reactor.

Catalyst	CO conversion (%)	Hydrocarbon selectivity (wt%)					Chain growth probability (α)[a]
		C_1	C_2–C_4	C_{10}–C_{20}	C_{21+}	C_{5+}	
Co/TiO_2	84.6	4.6	5.4	36.5	29.9	90.0	0.89

[a] Calculated within the range of C_{10}–C_{22}.

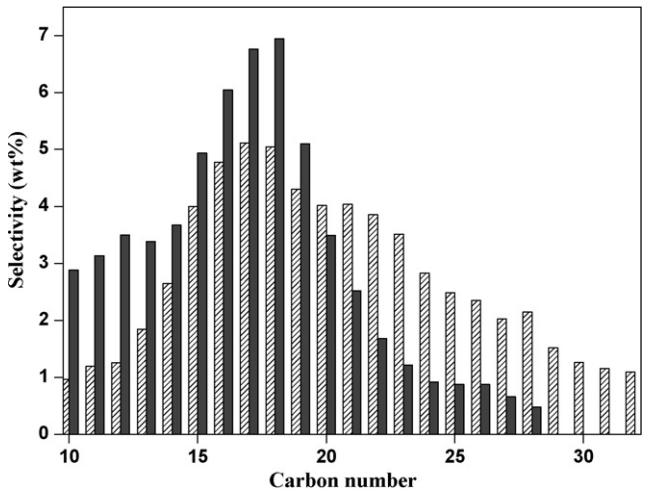

Fig. 4. Carbon number distributions in the first-bed reactor and in the dual-bed reactor ((▨) Co/TiO_2 (first-bed only), (■) CO/TiO_2 (first-bed) + Pd/XA800 (second-bed)).

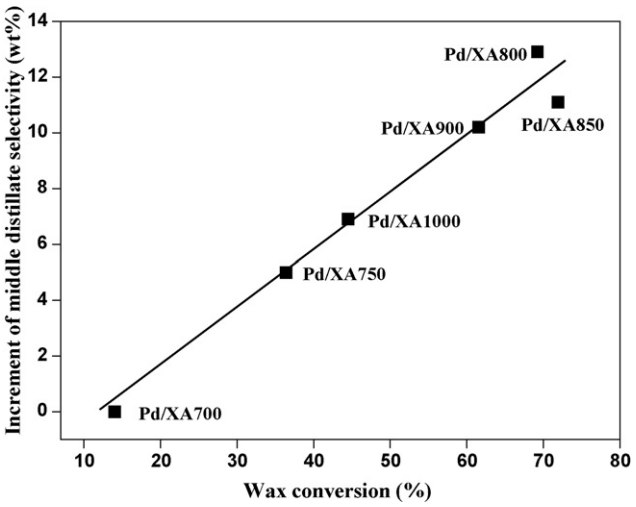

Fig. 5. A correlation between wax conversion and increment of middle distillate selectivity in the second-bed reactor.

dle distillate selectivity by the selective hydrocracking of wax over Pd/XA800 catalyst.

Carbon number distributions over Pd/XA catalysts are summarized in Table 3. Selectivities for methane and light hydrocarbons (C_2–C_4) in the dual-bed reactor were somewhat increased compared to those in the first-bed reactor, indicating the occurrence of hydrocracking in the second-bed reactor. It is noticeable that selectivity for middle distillate over Pd/XA750, Pd/XA800, Pd/XA850, Pd/XA900, and Pd/XA1000 catalysts in the dual-bed reactor considerably increased compared to that in the first-bed reactor. On the other hand, selectivity for middle distillate over Pd/XA700 catalyst in the dual-bed reactor was almost identical to that in the first-bed reactor. This result may be due to the fact that a little amount of wax was hydrocracked and small amount of middle distillate was produced over Pd/XA700 catalyst, and furthermore, middle distillate was also hydrocracked to gasoline and gaseous hydrocarbons over Pd/XA700 catalyst. In other words, conversion of wax and selectivity for middle distillate over Pd/XA700 catalyst did not change significantly, indicating that Pd/XA700 catalyst was not efficient as a second-bed catalyst.

Fig. 5 shows the correlation between wax conversion and increment of middle distillate selectivity in the second-bed reactor. Wax conversion and increment of middle distillate selectivity were calculated according to the following equations. It is noticeable that the increment of middle distillate selectivity increased with increasing wax conversion. This indicates that the increment of the middle distillate selectivity was mainly due to the hydrocracking of wax. The increment of middle distillate selectivity was attributed to the second-bed catalysis. This implies that the formation of middle distillate by hydrocracking of wax strongly depended on the characteristics of second-bed catalyst:

$$\text{Wax conversion (\%)} = \frac{29.9\,\text{wt\% (wt\% of wax formed in the first-bed reactor)} - (\text{wt\% of wax remained in the second-bed reactor})}{29.9\,\text{wt\% (wt\% of wax formed in the first-bed reactor)}} \times 100 \quad (3)$$

$$\text{Increment of middle distillate selectivity (wt\%)} = (\text{wt\% of middle distillate in the second-bed reactor}) - 36.5\,\text{wt\% (wt\% of middle distillate formed in the first-bed reactor)} \times 100 \quad (4)$$

Fig. 6 shows the correlation between calcination temperature of XA support and increment of middle distillate selectivity in the second-bed reactor. Interestingly, the increment of middle distillate selectivity showed a volcano-shaped curve with respect to calcination temperature of XA support. Among the catalysts tested,

Table 3
Carbon number distributions over Pd/XA catalysts in the second-bed reactor.

Catalyst	Hydrocarbon selectivity (wt%)				
	C_1	C_2–C_4	C_{10}–C_{20}	C_{21+}	C_{5+}
Pd/XA700	9.6	8.2	36.3	25.7	82.2
Pd/XA750	11.8	7.1	41.5	19.0	81.1
Pd/XA800	10.8	10.4	49.4	9.2	78.8
Pd/XA850	13.8	10.4	47.6	8.4	75.8
Pd/XA900	9.1	11.3	46.7	11.5	79.6
Pd/XA1000	6.8	11.5	43.4	16.6	81.7

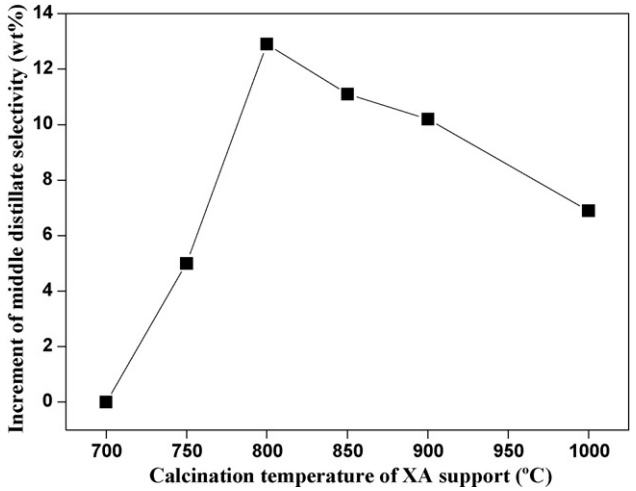

Fig. 6. A correlation between calcination temperature of XA support and increment of middle distillate selectivity in the second-bed reactor.

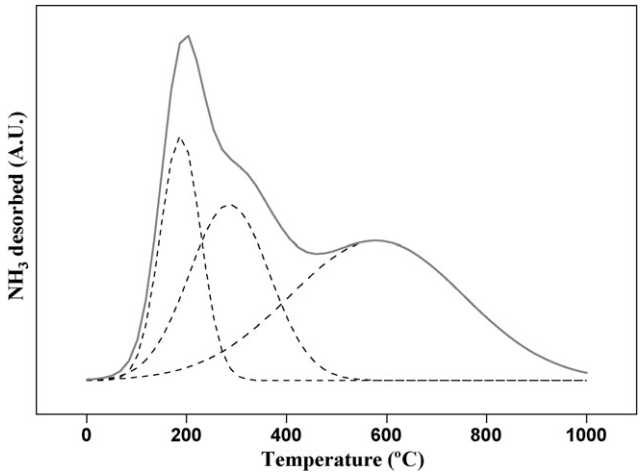

Fig. 7. NH_3-TPD profile of Pd/XA800 catalyst.

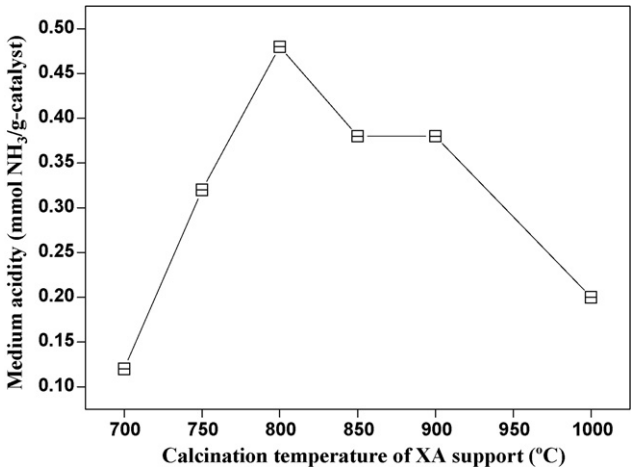

Fig. 8. A correlation between calcination temperature of XA support and medium acidity of Pd/XA catalyst.

Pd/XA800 catalyst showed the highest increment of middle distillate selectivity. Therefore, acid properties of Pd/XA catalysts were examined to elucidate the different catalytic performance of Pd/XA catalysts in the second-bed reactor.

3.4. Effect of acid property of Pd/XA catalysts

In order to investigate the effect of acid properties of Pd/XA catalysts on their catalytic performance in the second-bed reactor, NH_3-TPD measurements were conducted. Fig. 7 shows the NH_3-TPD profile of Pd/XA800 catalyst. Deconvolution of the TPD profile reveals that there are three types of acid sites. A low-temperature peak in the range of 170–240 °C, a medium-temperature peak in the range of 270–330 °C, and a high-temperature peak in the range of 560–700 °C correspond to weak, medium, and strong acid sites, respectively. All the other Pd/XA catalysts also showed three types of acid sites. Acidities of Pd/XA catalysts are summarized in Table 4. The result shows that Pd/XA catalysts retained different total acidity depending on the calcination temperature of XA support. In particular, total acidity of Pd/XA1000 catalyst was much lower than that of the other Pd/XA catalysts. The small total acidity of Pd/XA1000 catalyst was attributed to the small surface area and high degree of crystallization of alumina support. It is generally accepted that γ-Al_2O_3 is more acidic than δ-, θ-, and α-Al_2O_3, and consequently, is more active for many acid-catalyzed reactions [2,16,35]. As shown in Fig. 3, boehmite was gradually transformed to γ-Al_2O_3 at calcination temperature above 700 °C, and fully developed γ-Al_2O_3 started to appear after calcinations at 750 °C. After high-calcination temperature of 1000 °C, on the other hand, alumina lost most of acid property by forming δ-, θ-, or α-Al_2O_3 phase with high crystallinity. It was observed that the strong acidity decreased with increasing calcination temperature, indicating that the strong acid site is closely related to the surface area or degree of crystallization of the support.

As described earlier, the acid property of Pd/XA catalyst may play an important role in the hydrocracking of wax. Fig. 8 shows the correlation between calcination temperature of XA support and medium acidity of Pd/XA catalyst. The medium acidity of Pd/XA catalyst showed a volcano-shaped curve with respect to calcination temperature of XA support. This trend is well consistent with the trend of increment of middle distillate selectivity in the second-bed reactor with respect to calcination temperature of XA support (Fig. 6). This indicates that the increment of middle distillate selectivity is closely related to the medium acidity of Pd/XA catalyst. It has been reported that the medium acidity is directly related to the surface reactivity of alumina [33]. This implies that the medium acidity of Pd/XA catalyst plays a crucial role in the hydrocracking of wax.

Many attempts have been made in order to correlate the acid property with the wax hydrocracking activity of Pd/XA catalyst. It was found that weak acidity, strong acidity, and total acidity showed no reliable correlation with the wax hydrocracking activity of Pd/XA catalyst. However, a reliable correlation between medium acidity and wax hydrocracking ability of Pd/XA catalyst was observed. Fig. 9 shows the correlation between medium acidity of Pd/XA catalyst and increment of middle distillate selectivity in the second-bed reactor. The increment of middle distillate selectivity in the second-bed reactor was roughly increased with increasing medium acidity of Pd/XA catalyst. This result is well consistent with the previous reports [12,22,39–43]. The above result is also well supported by the hydrocracking process, where activation of the paraffin reactant occurs by the bifunctional hydrocracking mechanism (by dehydrogenation on the metal sites followed by protonation of the olefin on the Brønsted acid sites of acidic support). Therefore, the amount of acid sites of supporting material serves as a crucial factor in many hydro-conversion reactions such as hydrocracking, hydroisomerization, and transalkylation. In particular, it is known that conversions of hydrocarbons in the hydro-conversion reactions are

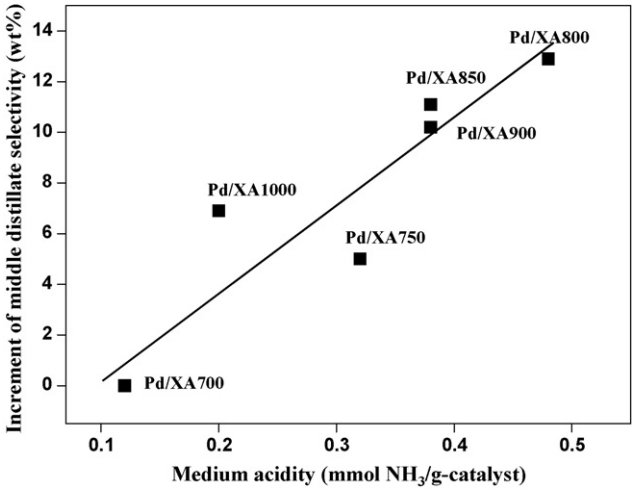

Fig. 9. A correlation between medium acidity of Pd/XA catalyst and increment of middle distillate selectivity in the second-bed reactor.

Table 4
Acidities of Pd/XA catalysts.

Catalyst	Acidity (mmol NH_3/g-catalyst)			
	Weak acid site (170–240 °C)	Medium acid site (270–330 °C)	Strong acid site (560–700 °C)	Total acidity
Pd/XA700	0.41	0.12	0.94	1.47
Pd/XA750	0.28	0.32	0.80	1.40
Pd/XA800	0.37	0.48	0.78	1.63
Pd/XA850	0.33	0.38	0.74	1.45
Pd/XA900	0.38	0.38	0.68	1.44
Pd/XA1000	0.14	0.20	0.18	0.52

mainly related to the amount of medium acid sites [44,45]. All these strongly support our conclusion that the medium acidity served as a crucial factor in the hydrocracking of wax over Pd/XA catalyst. Among the Pd/XA catalysts, Pd/XA800 catalyst with the highest medium acidity showed the best catalytic performance in the hydrockacking of wax (Tables 3 and 4, Figs. 5 and 9). The Pd/XA800 catalyst exhibited 12.9 wt% increment of middle distillate selectivity, when compared to the effluent stream from the first-bed reactor.

3.5. Catalyst stability

The reaction system examined in this work is composed of two catalytic reactions; (i) synthesis of hydrocarbons through Fischer–Tropsch synthesis in the first-bed reactor and (ii) hydrocracking of produced hydrocarbons in the second-bed reactor. Because both reactions are involved in our reaction system, it is very difficult to definitely say that which reaction dominantly results in catalyst deactivation. In other words, the catalyst deactivation of dual-bed reaction system is not caused by only the second-bed catalyst, because Co/TiO_2 catalyst can also experience catalyst deactivation. It was observed that selectivities for methane, light hydrocarbon gases (C_2–C_4), middle distillate, and wax over Co/TiO_2 + Pd/XA800 catalysts after 24-h reaction were 18.05, 12.55, 38.23, and 2.32 wt%, respectively. This result implies that chain growth probability over the first-bed catalyst (Co/TiO_2) was decreased, resulting in remarkable increase of methane selectivity and decrease of middle distillate selectivity. Therefore, stability of Pd/XA catalyst under our reaction conditions was discussed on the basis of changes in textural properties.

In order to ensure the catalyst stability, nitrogen adsorption–desorption measurements were conducted before and after the reaction. Fig. 10 shows the nitrogen adsorption–desorption isotherms of Pd/XA800 catalyst obtained before and after the reaction (24-h reaction at 12 bar and 330 °C). The Pd/XA800 catalyst showed very similar isotherms before and after the reaction. Surface areas, pore volumes, and average pore diameters of Pd/XA800 catalyst before and after the reaction are listed in Table 5. Surface area of the catalyst was slightly decreased after the reaction because the catalyst was annealed during the long reaction time (24 h). However, no significant changes in pore volume and average pore diameter were observed before and after the reaction. This indicates that Pd/XA800 served as a stable catalyst in the hydrockacking of wax performed at high pressure and temperature.

Table 5
Textural properties of Pd/XA800 catalyst before and after the reaction (24-h reaction).

Pd/XA800 catalyst	Surface area ($m^2\ g^{-1}$)[a]	Pore volume ($cm^3\ g^{-1}$)[b]	Average pore diameter (nm)[c]
Before reaction	188	0.50	7.4
After reaction	153	0.42	7.6

[a] Calculated by the BET equation.
[b] BJH desorption pore volume.
[c] BJH desorption average pore diameter.

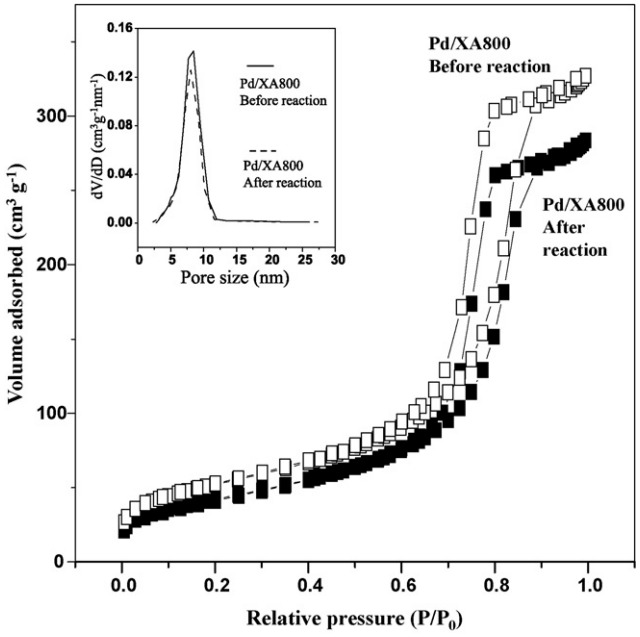

Fig. 10. Nitrogen adsorption–desorption isotherms and pore size distributions of Pd/XA800 catalyst before and after the reaction (24-h reaction).

4. Conclusions

Selective production of middle distillate (C_{10}–C_{20}) from synthesis gas ($CO + H_2$) through wax hydrocracking was carried out in a dual-bed reactor. Co/TiO_2 catalyst prepared by an incipient wetness impregnation method was used in the first-bed reactor to produce wax (C_{21+}) from synthesis gas, and Pd/XA catalysts prepared by an impregnation method were used in the second-bed reactor to produce middle distillate through wax hydrocracking. The effect of calcination temperature of XA supports on the wax hydrocracking performance of Pd/XA catalysts in the second-bed reactor was investigated. Co/TiO_2 catalyst in the first-bed reactor produced more than 35 wt% middle distillate and more than 25 wt% wax, which was suitable as a feed for the second-bed reactor. NH_3-TPD experiments revealed that all the Pd/XA catalysts retained three types of acid sites (weak, medium, and strong acid sites). It was found that the increment of middle distillate selectivity in the second-bed reactor and the medium acidity of Pd/XA catalyst showed volcano-shaped curves with respect to calcination temperature of XA support. More importantly, the increment of middle distillate selectivity increased with increasing medium acidity of Pd/XA catalyst, indicating that the medium acidity of Pd/XA catalyst played a very important role in determining the wax hydrocracking performance of Pd/XA catalyst. Among the Pd/XA catalysts,

Pd/XA800 catalyst with the highest medium acidity showed the best catalytic performance in the hydrocracking of wax (ca. 13 wt% increment of middle distillate selectivity).

Acknowledgements

The authors would like to acknowledge the financial support of KEMCO and GTL Technology Development Consortium (Korea National Oil Corp., Daelim Industrial Co. Ltd., Doosan Mecatec Co. Ltd., Hyundai Engineering Co. Ltd., and SK Energy Co. Ltd.) under "Energy & Resources Technology Development Programs" of the Ministry of Knowledge Economy, Republic of Korea (2006-11-0133-3-020).

References

[1] R. de Haan, G. Joorst, E. Mokoena, C.P. Nicolaides, Appl. Catal. A 327 (2007) 247–254.
[2] J. Scherzer, A.J. Gruia, Hydrocracking Science and Technology, Marcel Dekker, New York, 1996.
[3] G. Valavarasu, M. Bhaskar, K.S. Balaraman, Petrol. Sci. Technol. 21 (2003) 1185–1205.
[4] Z.-W. Liu, X. Li, K. Asami, K. Fujimoto, Catal. Today 104 (2005) 41–47.
[5] A. Shamsi, V.U.S. Rao, R.J. Gormely, R.T. Obermyer, R.R. Schehl, J.M. Stencel, Appl. Catal. 27 (1986) 55–68.
[6] F.G. Botes, W. Böhringer, Appl. Catal. A 267 (2004) 217–225.
[7] Y. Yoneyma, J. He, Y. Morii, S. Azuma, N. Tsubaki, Catal. Today 104 (2005) 37–40.
[8] Z.-W. Liu, X. Li, K. Asami, K. Fujimoto, Energy Fuels 19 (2005) 1790–1794.
[9] F.G. Botes, Appl. Catal. A 284 (2005) 21–29.
[10] S.T. Sie, M.M.G. Senden, H.M.H. van Wechem, Catal. Today 8 (1991) 371–394.
[11] S.T. Sie, Ind. Eng. Chem. Res. 32 (1993) 403–408.
[12] K.M. Cho, S. Park, J.G. Seo, M.H. Youn, S.-H. Baeck, K.-W. Jun, J.S. Chung, I.K. Song, Appl. Catal. B 83 (2008) 195–201.
[13] A.Y. Khodakov, W. Chu, P. Fongarland, Chem. Rev. 107 (2007) 1692–1744.
[14] H. Schulz, Appl. Catal. A 186 (1999) 3–12.
[15] A. Martínez, C. Lopez, Appl. Catal. A 294 (2005) 251–259.
[16] V. Udaya, S. Rao, R.J. Gormley, Catal. Today 6 (1990) 207–234.
[17] J. Eilers, S.A. Posthuma, S.T. Sie, Catal. Lett. 7 (1990) 253–270.
[18] J.A. Brennan, P.D. Caesar, J.C. Pitman, W.E. Garwood, US Patent 4,304,871 (1981).
[19] W.O. Haag, T.J. Huang, US Patent 4,159,995 (1979).
[20] W.O. Haag, T.J. Huang, US Patent 4,279,830 (1981).
[21] S. Bessell, Appl. Catal. A 126 (1995) 235–244.
[22] Y. Rezgui, M. Guemini, Appl. Catal. A 282 (2005) 45–53.
[23] K. Fang, W. Wei, F. Ren, Y. Sun, Catal. Lett. 93 (2004) 235–242.
[24] S. Mohanty, D. Kunzru, D.N. Saraf, Fuel 69 (1990) 1467–1473.
[25] M.E. Dry, Appl. Catal. A 189 (1999) 185–190.
[26] J. Grunes, J. Zhu, M. Yang, G.A. Somorjai, Catal. Lett. 86 (2003) 157.
[27] K. Balakrishnan, R.D. Gonzalez, J. Catal. 144 (1993) 395–413.
[28] L. Hu, K.A. Boateng, J.M. Hill, J. Mol. Catal. A 259 (2006) 51–60.
[29] J.G. Seo, M.H. Youn, K.M. Cho, S. Park, I.K. Song, J. Power Sources 173 (2007) 943–949.
[30] J.G. Seo, M.H. Youn, H.-I. Lee, J.J. Kim, E. Yang, J.S. Chung, P. Kim, I.K. Song, Chem. Eng. J. 141 (2008) 298–304.
[31] S.H. Cai, S.N. Rashkeev, S.T. Pantelides, K. Sohlberg, Phys. Rev. B 67 (2003) 224104.
[32] H.C. Stumpf, A.S. Russell, J.W. Newsome, C.M. Tucker, Ind. Eng. Chem. 42 (1950) 1398–1403.
[33] G.S. Walker, D.R. Pyke, C.R. Werrett, E. Williams, A.K. Bhattacharya, Appl. Surf. Sci. 147 (1999) 228–234.
[34] N.N. Madikizela-Mngangeni, N.J. Coville, J. Mol. Catal. A 225 (2005) 137–142.
[35] G.K. Chuah, S. Jaenicke, T.H. Xu, Micropor. Mesopor. Mater. 37 (2000) 345–353.
[36] K. Maeda, F. Mizukami, M. Watanabe, N. Arai, S. Niwa, M. Toba, K. Shimizu, J. Mater. Sci. Lett. 9 (1990) 522–523.
[37] Z.-X. Sun, T.-T. Zheng, Q.B. Bo, M. Du, W. Forsling, J. Colloid Interf. Sci. 319 (2008) 247–251.
[38] C. Kaya, F. Kaya, A.R. Boccacconi, K.K. Chawla, Acta Mater. 49 (2001) 1189–1197.
[39] X. Lin, Y. Fan, Z. Liu, G. Shi, H. Liu, X. Bao, Catal. Today 125 (3–4) (2007) 185–191.
[40] Y. Fan, X. Bao, G. Shi, W. Wei, J. Xu, Appl. Catal. A 275 (2004) 61–71.
[41] A.R. Songip, T. Masuda, H. Kuwahara, K. Hashimoto, Energy Fuels 8 (1994) 131–135.
[42] T. Masuda, H. Kuwahara, S.R. Mukai, K. Hashimoto, Chem. Eng. Sci. 54 (1999) 2773–2779.
[43] A.R. Songip, T. Masuda, H. Kuwahara, K. Hashimoto, Energy Fuels 8 (1994) 136–140.
[44] K. Wang, X. Wang, G. Li, Catal. Commun. 8 (3) (2007) 324–328.
[45] L. Liu, M. Cheng, D. Ma, G. Hu, X. Pan, X. Bao, Micropor. Mesopor. Mater. 94 (2006) 304–312.